

1 **The Impact of Increasing Stratospheric Radiative Damping on the QBO Period**

2 Tiehan Zhou^{1,2}, Kevin DallaSanta^{1,3}, Larissa Nazarenko^{1,2}, Gavin A. Schmidt¹, Zhonghai Jin¹

3 ¹NASA Goddard Institute for Space Studies, New York, NY

4 ²Center for Climate Systems Research, Columbia University, New York, NY

5 ³Universities Space Research Association, Columbia, MD

6
7 Correspondence to: Tiehan Zhou (tz2131@columbia.edu)

8
9 **Abstract.** Stratospheric radiative damping increases as atmospheric carbon dioxide concentration rises.
10 We use the one-dimensional mechanistic models of the QBO to conduct sensitivity experiments and
11 find that the simulated QBO period shortens due to the enhancing of radiative damping in the
12 stratosphere. This result suggests that increasing stratospheric radiative damping due to rising CO₂ may
13 play a role in determining the QBO period in a warming climate along with wave momentum flux
14 entering the stratosphere and tropical vertical residual velocity, both of which also respond to
15 increasing CO₂.

16 17 **1. Introduction**

18 The quasi-biennial oscillation (QBO) dominates the variability of the equatorial middle and lower
19 stratosphere and is characterized by a downward propagating zonal wind regime that regularly changes
20 from westerlies to easterlies. The QBO period ranges from 22 to 34 months with its average being
21 slightly longer than 28 months. The QBO not only manifests itself in the equatorial zonal winds, but also
22 leaves an imprint on the temperature in both the tropics and extratropics (Baldwin et al., 2001 and
23 references therein).

24 The QBO has far-reaching implications for global weather and climate systems. First of all, the QBO
25 exerts a marked influence on the distribution and transport of various chemical constituents such as
26 ozone (O_3) (e.g., Hasebe, 1994), water vapor (H_2O) (e.g., Kawatani et al., 2014), methane (CH_4), nitrous
27 oxide (N_2O), hydrogen fluoride (HF), hydrochloric acid (HCl), odd nitrogen species (NO_y) (e.g.,
28 Zawodny and McCormick, 1991), and volcanic aerosol (Trepte and Hitchman, 1992). Secondly, it is
29 well appreciated that the QBO influences the extratropical circulation in the winter stratosphere, which
30 is commonly known as the Holton–Tan effect (Holton and Tan, 1980; Labitzke, 1982). It has been noted
31 that the effect of the QBO on the extratropical winter stratosphere impacts the severity of stratospheric
32 ozone depletion (e.g., Lait et al., 1989). Furthermore, taking account of the QBO improves the simulation
33 and predictability of the extratropical troposphere (e.g., Marshall and Scaife, 2009). Finally, through its
34 modulation of temperature and vertical wind shear in the vicinity of the tropical tropopause, the QBO
35 influences tropical moist convection (Collimore et al., 2003; Liess and Geller, 2012), the El Niño–
36 Southern Oscillation (ENSO) (Gray et al., 1992; Huang et al., 2012; Hansen et al. 2016), the Hadley
37 circulation (Hitchman and Huesmann, 2009), the tropospheric subtropical jet (Garfinkel and Hartmann,
38 2011a, 2011b), the boreal summer monsoon (Giorgetta et al., 1999), and the Madden-Julian Oscillation
39 (Yoo and Son, 2016). Intriguingly, the QBO is also reported to influence the activities of tropical
40 cyclones (Gray et al., 1984; Ho et al., 2009), albeit this issue is still unsettled (Camargo and Sobel, 2010)
41 and needs further study.

42 Efforts to understand and simulate the QBO have been ongoing ever since its discovery by Ebdon
43 (1960) and Reed et al. (1961). Lindzen and Holton (1968) and Holton and Lindzen (1972) developed
44 the classical theory of the QBO. Namely, as waves propagate upward, they are attenuated by thermal
45 damping, encounter critical levels, and accelerate and decelerate the mean flow, providing momentum
46 sources for both the westerly and easterly phases of the QBO.

47 Holton and Lindzen's (1972) model (hereafter referred to as HL model) was further simplified by
48 Plumb (1977), the elegance of which made it a standard paradigm for the QBO. In Plumb's (1977)
49 Boussinesq formulation, the QBO period is inversely dependent upon both the momentum flux and
50 thermal dissipation rate. Hamilton (1981) further highlighted the role of the radiative damping rate on
51 both the realistic vertical structure and the realistic period of the QBO.

91 By adopting higher vertical resolutions and incorporating various gravity wave parameterization
92 schemes, many state-of-the-art climate models have shown the capability to self-consistently simulate
93 the QBO (Scaife et al., 2000; Giorgetta et al., 2002, 2006; Rind et al., 2014, 2020; Geller et al., 2016a;
94 Richter et al., 2020a, 2020b). Given the important implications of the QBO for the global climate system,
95 it is natural to ask how the QBO will change in a warming climate.

96 Giorgetta and Doege (2005) showed a shortening of the QBO period in their doubled CO₂
97 experiments. They reasoned that both the weakening of the tropical upwelling and the prescribed
98 increase of gravity wave sources lead to the reduction of the QBO period in a warming climate. However,
99 most climate models project a strengthening rather than weakening of tropical upwelling in a warmer
100 climate (Butchart et al., 2006; Butchart 2014; Li et al., 2008). Employing a model without any
101 parametrized non-orographic gravity waves, Kawatani et al. (2011) demonstrated that the intensifying
102 tropical upwelling in a warming climate dominates the counteracting effect of enhanced wave fluxes and
103 consequently projected a lengthening of the QBO period. Using fixed sources of parametrized gravity
104 waves, Watanabe and Kawatani (2012) also projected an elongation of the QBO period in a warming
105 climate and ascribed it to the stronger tropical upwelling. Analyzing four Coupled Model
106 Intercomparison Project phase 5 (CMIP5) models that could simulate a reasonable QBO, Kawatani and
107 Hamilton (2013) found that the projected trends of the QBO period were inconsistent in sign. They
108 further investigated the 60-year operational balloon-borne radiosonde observations provided by the Free

109 Berlin University and detected no significant trend in the QBO period. Richter et al. (2020b) investigated
110 the response of the QBO to doubled and quadrupled CO₂ climates among eleven models that participated
111 in Phase 1 of the Stratospheric-tropospheric Processes And their Role in Climate QBO-initiative (QBOi;
112 Butchart et al., 2018), and found no consensus on how the QBO period would respond to a changing
113 climate. Recently, Butchart et al. (2020) evaluated ten Coupled Model Intercomparison Project phase 6
114 (CMIP6) models with realistic QBO in two Shared Socioeconomic Pathways (SSPs, Gidden et al., 2019)
115 scenario simulations and surprisingly found that the QBO period shortens in seven of those ten models
116 in both in both SSP3-7.0 and SSP5-8.5 scenarios although only two and three models show a significant
117 shortening trend in the respective scenarios.

118 It is challenging to ascertain the trend of the QBO period in a warming climate. On one hand, a
119 speeding-up of the Brewer-Dobson circulation in a warming climate leads to a lengthening of the QBO
120 period in most climate models. On the other hand, there is a robust increase in the vertical component of
121 the EP flux for both eastward and westward propagating waves (Richter et al., 2020b; Butchart et al.,
122 2020), indicating that the QBO period shortens due to the enhanced wave driving in a warming climate.
123 The competing effects between enhanced wave driving and a faster Brewer-Dobson circulation suggests
124 that trends in the QBO period are likely to be small and difficult to detect due to the large cycle-to-cycle
125 variability that is reproduced by climate models (Butchart et al., 2020). In addition, uncertainty in the
126 representation of the parameterized gravity waves make it more elusive to detect the trend of the QBO
127 period in a warming climate (Schirber et al., 2015; Richter et al., 2020b).

128 Given the fact that the QBO period is influenced by the radiative damping (Plumb 1977; Hamilton
129 1981), a natural question to ask is whether it could play a role on the trend of the QBO in a warming
130 climate. Plass (1956) showed that when the CO₂ concentration is increased from 330 ppmv to 660 ppmv,
131 the cooling rate increases significantly in the middle and upper stratosphere while it is not changed below

132 the 24 km height level. The cooling rate is increased by about 50% around the 40 km height level (see
133 his Figure 8).

134 It is well-known that enhanced wave fluxes entering the stratosphere and stronger tropical upwelling
135 individually play a dominant role in determining the trends in the QBO period in a warming climate.
136 Does the competing effect between them leave some room for increasing stratospheric radiative damping
137 to exert an influence on the QBO period? In this paper, we use the HL model to isolate the effect of
138 radiative damping on the QBO period by assuming that the momentum flux entering the stratosphere
139 doesn't change in our experiments. Observational and modeling studies (Andrews et al., 1987; Kawatani
140 et al., 2009, 2010, 2011; Richter et al., 2020b; Holt et al., 2020) showed that the wave forcing spectrum
141 is similar to a discrete two-wave spectrum rather than red-noise or white-noise, all of which are
142 illustrated in Saravanan (1990). Accordingly, the QBO is indeed sensitive to stratospheric radiative
143 damping, and the HL model is suitable for us to conduct the sensitivity analysis.

144 The remainder of this paper is organized as follows. Section 2 investigates the sensitivity of the QBO
145 period to the radiative damping using HL's original model. Section 3 explores the sensitivity of the QBO
146 period to the radiative damping using a modified HL model where the semiannual forcing is removed.
147 Discussion and conclusions are presented in Sections 4 and 5 respectively.

148

149 **2. Sensitivity of the QBO period to enhanced stratospheric radiative damping in the original HL** 150 **model**

151 In the HL model the governing equation of mean flow emerges after the primitive momentum
152 equation is meridionally averaged over some suitable latitudinal belt over the equator.

$$153 \quad \frac{\partial \bar{u}}{\partial t} = -\frac{1}{\rho_0} \frac{\partial}{\partial z} \left[\sum_{i=0}^1 \bar{F}_i \right] + K_z \frac{\partial^2 \bar{u}}{\partial z^2} + G \quad (1)$$

154 where \bar{u} is mean zonal wind, ρ_0 is mean density, \bar{F}_i is the meridionally averaged vertical Eliassen-Palm
 155 flux associated with wave i , the index i refers to the individual waves, K_z is a vertical eddy diffusion
 156 coefficient, t is time, z is altitude, and G is semiannual forcing identical to that specified by HL.

157 The \bar{F}_i is are evaluated with Lindzen's (1971) WKB formalism for equatorial waves in shear. When
 158 only infrared cooling acts to damp the waves the formulae for \bar{F}_i are

$$159 \quad \bar{F}_0(z) = A_0 \exp \left(- \int_{17km}^z \frac{\alpha N}{k(c - \bar{u})^2} dz \right) \quad (2)$$

160 for the Kelvin wave, and

$$161 \quad \bar{F}_1(z) = A_1 \exp \left[- \int_{17km}^z \frac{\alpha \beta N}{k^3(c - \bar{u})^3} \left(1 - \frac{k^2(\bar{u} - c)}{\beta} \right) dz \right] \quad (3)$$

162 for the mixed Rossby-gravity wave. As in HL, the wavenumber k , the phase speed c , and A_0 are chosen
 163 to be $2\pi/(40,000 \text{ km})$, 30 m s^{-1} , and $0.04 \text{ m}^2 \text{ s}^{-2} \rho_0(17 \text{ km})$, respectively for the Kelvin wave while
 164 they are equal to $-2\pi/(10,000 \text{ km})$, -30 m s^{-1} , and $-0.04 \text{ m}^2 \text{ s}^{-2} \rho_0(17 \text{ km})$, respectively for the
 165 mixed Rossby-gravity wave. In Eq. (1), $K_z = 0.3 \text{ m}^2 \text{ s}^{-1}$, which is also the same as in HL. In addition,
 166 $\beta = 2\Omega/a$, where Ω is earth's rotation rate, and a is earth's radius. HL's boundary conditions stipulated
 167 that $\bar{u} = 0$ at the lowest model level (17 km) and constrained \bar{u} to vary semiannually at the top level (35
 168 km).

169 In our control run that is used to depict the present-day QBO all the model parameters are identical
 170 to those used by HL in their original simulation. The Brunt-Väisälä frequency

$$171 \quad N = \sqrt{\frac{g}{T_0} \left(\frac{dT_0}{dz} + \frac{g}{c_p} \right)} \quad (4)$$

172 In Eq. (4), g is gravity, T_0 is mean temperature, and c_p is specific heat of dry air at constant pressure.
 173 HL set N in Eq. (4) to $2.16 \times 10^{-2} \text{ s}^{-1}$ with a scale height $H = 6 \text{ km}$. In addition, the Newtonian

cooling profile in our control run, i.e., $\alpha(z)$ in Eqs. (2) and (3), is also identical to that in the original HL model and depicted in FIG. 1a as the black line. Namely, $\alpha(z)$ in the control run increases from $(21 \text{ day})^{-1}$ at 17 km to $(7 \text{ day})^{-1}$ at 30 km and is kept at $(7 \text{ day})^{-1}$ between 30 km and 35 km. Fels (1985) explained why the magnitude of this radiative damping rate is suitable for simulating the QBO on the basis of the scale-dependent effect of radiative damping (Fels, 1982). Hamilton (1981) demonstrated that the proper choice of $\alpha(z)$ is crucial in simulating a realistic vertical structure of the QBO.

Eq. (1) was integrated for 100 years using the forward-backward scheme (Matsuno, 1966). The vertical resolution was 250 m and identical to that in HL. The time step was 12 hr, i.e., one half of used in HL, because the 24-hr time step resulted in numerical instability in our integration.

FIG. 2a shows the time–height section of the monthly averaged mean zonal wind simulated over the first 20 years using the HL model. Both the QBO and the semiannual oscillation (SAO) are conspicuous. The fast Fourier transform (FFT) method is used to calculate the frequency power spectra. In order to more accurately derive the QBO period, the model was run for 100 years to increase the spectral resolution. Frequency–height sections of the power spectral densities (PSD) over zero to the Nyquist frequency, i.e., 0.5 cycle/month, depict two sharp lines (peaks) at $\frac{1}{30}$ and $\frac{1}{6}$ cycle/month, respectively (not shown). In order to better visualize the magnitudes of the PSD, we show two truncated frequency–height sections with FIG. 2b and FIG. 2c highlighting the QBO and the SAO respectively. FIG. 2b shows that the QBO dominates over the model domain. The peak frequency corresponds to the period of 30 months. FIG. 2c shows the SAO dominates near the model top due to the fact a semiannual forcing was imposed in the altitudes from 28 to 35 km.

It is worth mentioning that the QBO period shown here is longer than 26.5 months reported in the HL paper (see their FIG. 1). Using the HL model parameters, the QBO period simulated by Plumb (1977)

197 was close to three years (refer to his FIG. 8a), which is longer than our simulated QBO period, i.e., 30.0
 198 months. Although we could not explain why our simulated QBO period is longer than that simulated by
 199 HL, we found that when the upper boundary condition is changed from $\bar{u} = 14 \sin(\omega_a t)$ and $\omega_a =$
 200 $\frac{2\pi}{180} \text{ day}^{-1}$ used in the HL's original model (refer to their Eqs. (2)) to $\frac{\partial \bar{u}}{\partial z} = 0$ used in Plumb (1977), the
 201 simulated QBO period becomes 34.3 month (figure not shown). In other words, when we adopted the
 202 stress-free upper boundary condition as in Plumb (1977), our simulated QBO period is comparable to
 203 that simulated by him, which lends credence to our reconstruction of the HL model.

204 As mentioned in Section 1, when the atmospheric carbon dioxide concentration is doubled the cooling
 205 rate increases significantly in the middle and upper stratosphere while it varies little below the 24 km
 206 height level. Accordingly, $\alpha(z)$ in the experimental run is kept the same as in the control run, i.e.,
 207 increases from $(21 \text{ day})^{-1}$ at 17 km to $\frac{9}{91} \text{ day}^{-1}$ at 24 km. Since the cooling rate is increased by about
 208 50% around the 40 km height level (Plass, 1956), the radiative damping rates are expected to also
 209 increase in the middle and upper stratosphere as the CO_2 concentration rises. However, the relative
 210 change of cooling rate Q in response to the increasing CO_2 is not identical to that of Newtonian cooling
 211 coefficient due to the facts that $Q = -\alpha(T - T_e)$ and the radiative equilibrium temperature T_e in the
 212 stratosphere decreases as the CO_2 concentrations increase (Manabe et al. 1967). In other words, for any
 213 given temperature profile as adopted by Plass (1956), the decreasing of the stratospheric T_e with
 214 increasing CO_2 concentration leads to $\alpha_2(z) : \alpha_1(z) \neq Q_2(z) : Q_1(z)$, where $\alpha_1(z)$ and $\alpha_2(z)$ represent
 215 the Newtonian cooling coefficient at any altitude z for the reference and doubled CO_2 , respectively while
 216 $Q_1(z)$ and $Q_2(z)$ stand for the cooling rate likewise. In order to rigorously quantify $\alpha_2(z) : \alpha_1(z)$, we
 217 follow Dickinson (1973) in using a radiative transfer model to calculate $Q_1(T)$ for a reference
 218 temperature profile $T(z)$ and $Q_1(T + \delta)$ for $T(z) + \delta$, where a small perturbation $\delta T = 0.1 \text{ K}$ with
 219 $T(z)$ being the 1976 U.S. standard atmosphere. Our radiative transfer computations use the MODTRAN

220 gas absorption database with 0.1 cm^{-1} spectral resolution (Jin et al. 2019; Berk et al. 2008). We then
 221 repeat the computations with the doubled CO_2 to yield $Q_2(T)$ and $Q_2(T + \delta)$. It follows that $\frac{\alpha_2}{\alpha_1} =$
 222 $\frac{Q_2(T+\delta) - Q_2(T)}{Q_1(T+\delta) - Q_1(T)}$. In FIG. 1b the black line depicts the ratio for the broadband longwave radiation ($5 \mu\text{m} -$
 223 $100 \mu\text{m}$) and the red line delineates the ratio for the CO_2 absorption band ($12 \mu\text{m} - 18 \mu\text{m}$) used by
 224 Plass (1956). For the CO_2 absorption band, the calculated ratio is evidently comparable to the ratio of
 225 cooling rates between the doubled CO_2 and the reference CO_2 shown in figure 8 of Plass (1956), with an
 226 additional small increase (<1.1) below the 24 km level. The ratio calculated over the broadband is
 227 conspicuously smaller than that for the CO_2 absorption band, because the changes in cooling rate from
 228 the temperature perturbation are larger over a wider spectral band.

229 Returning to the 1D HL model, we synthesize those findings by prescribing $\alpha_2(z)$ in our
 230 experimental runs for the doubled CO_2 as follows: an increase of 30% between 30 and 35 km, no change
 231 below 24 km, and linear interpolation between 24 and 30 km. The resulting increase of radiative damping
 232 rate from the control runs is depicted as the red line in FIG. 1a. This increase is reasonable based on our
 233 results shown in FIG. 1b.

234 FIG. 3a shows the time–height section of the monthly averaged mean zonal wind simulated over the
 235 first 20 years for the doubled CO_2 run, where the increased $\alpha(z)$ depicted as the red line in FIG. 1a was
 236 employed while all other parameters are identical to those in the control run. Obviously, the QBO
 237 dominates below 28 km while the semiannual oscillation (SAO) dominates above 31 km. Like FIG. 2b
 238 and FIG. 2c, we only show two truncated frequency–height sections with FIG. 3b highlighting the QBO
 239 and FIG. 3c highlighting the SAO. FIG. 3b also shows that the QBO prevails over the model domain. The
 240 peak frequency corresponds to the period of 27.9 months. FIG. 3c shows the SAO dominates near the
 241 model top due to the same imposed semiannual forcing as that in the control run.

242 In summary, using the original HL model we found that the increased radiative damping due to the
243 doubling of CO₂ shortens the QBO period by 7% (i.e., decreases from 30 months to 27.9 months).

244

245 **3. Sensitivity of the QBO period to enhanced stratospheric radiative damping in the modified HL** 246 **model without the semiannual forcing**

247 HL pointed out that the imposed semiannual oscillation was not essential for their QBO theory.
248 Applying $\frac{\partial \bar{u}}{\partial z} = 0$ as the upper boundary condition, Plumb (1977) showed a simulated QBO without
249 resorting to the semiannual momentum source (refer to his FIG. 8b). In the following control run, all
250 parameters are identical to those used in the previous control run in Section 2 except that G in Eq. (1) is
251 set to zero with $\frac{\partial \bar{u}}{\partial z}$ also being set to zero at $z = 35$ km. Hereafter we refer to it as the Plumb model¹. FIG.
252 4a shows the time–height section of the monthly averaged mean zonal wind simulated over the first 20
253 years using the Plumb model. As expected, the QBO emerges without any trace of SAO since $G = 0$ in
254 Eq. (1). FIG. 4b shows that the QBO dominates over the whole model domain. The peak frequency
255 corresponds to the period of 37.5 months, which is comparable to that simulated by Plumb (1977) shown
256 in his FIG. 8b. Apparently, the QBO period from the Plumb model, i.e., 37.5 months shown in FIG. 4b,
257 is longer than that from the HL model, i.e., 30.0 months shown in FIG. 2b. This is partly because the
258 additional forcing G in Eq. (1) was removed in the Plumb model.

259 In the following experimental run, all parameters are identical to those used in the previous
260 experimental run in Section 2 except that G in Eq. (1) is set to zero with $\frac{\partial \bar{u}}{\partial z}$ also being set to zero at $z =$
261 35 km. In other words, the following experimental run using the Plumb model employed the same

¹ Strictly speaking, it is the HL model modified by Plumb (1977). In this paper, we don't use his eponymous model, i.e., the simplest possible model of the QBO, where Boussinesq fluids with uniform mean density were employed, because the HL model and its variant are considerably more realistic.

parameters as the afore-mentioned control run using the Plumb model except that the increased $\alpha(z)$ shown as the red line in FIG. 1a was used in the following experimental run while $\alpha(z)$ shown as the black line in FIG. 1a was used in the above control run. FIG. 5a shows the time–height section of the monthly averaged mean zonal wind simulated over the first 20 years for the doubled CO₂ run. It is natural that only the QBO emerges. A comparison of FIG. 4a and FIG. 5a shows that the QBO period shortens when the infrared damping increases in response to the doubled CO₂. FIG. 5b shows that the QBO dominates over the whole model domain. The peak frequency corresponds to the period of 31.6 months.

Using the Plumb model, we found that the increased radiative damping due to the doubling of CO₂ shortens the QBO period by 15.7% (i.e., decreases from 37.5 months to 31.6 months).

271

272 4. Discussion

Dunkerton (1997) showed that in the presence of tropical upwelling it was gravity waves rather than large-scale Kelvin and mixed Rossby-gravity waves that contributed the bulk of QBO forcing. Consequently, Geller et al. (2016a, 2016b) pointed out that enough gravity wave momentum flux is required to model the QBO in a self-consistent manner in climate models and that the magnitude of the subgrid-scale gravity wave momentum flux plays a crucial role in determining the QBO period. Since there is no tropical upwelling in either the HL model or the Plumb model, it is natural that planetary-scale Kelvin and mixed Rossby-gravity waves largely determine the QBO periods shown in Sections 2 and 3 due to the fact that the specified G is significantly weaker than that in the terrestrial stratosphere. We conducted another sensitivity test where all parameters are identical to those in the HL model except that G in both the control and experimental runs is twice as large as that used by HL. As the radiative damping profile changes from the black line to the red line above 24 km shown in FIG. 1a, our simulated QBO period decreases from 28.6 months to 27.3 months (figures not shown). This smaller percentage

285 decrease of 4.5% is not unexpected because G is not sensitive to the radiative damping at all and the
286 greater specified G reduces the fraction of the total wave forcing arising from the planetary waves.

287 We further conducted two sensitivity tests where all parameters are identical to those in the HL model
288 except that G in the first test is half as large as that used by HL and is equal to zero in the second test.
289 Surprisingly, as the radiative damping profile changes from the black line to the red line above 24 km
290 shown in FIG. 1a, our simulated QBO periods decreases from 30.0 months to 28.6 months both for G
291 being decreased by 50% and for $G = 0$ (figures not shown). This 4.7% decrease in the QBO period is
292 smaller than the 7% reduction obtained from the sensitivity test presented in Section 2 when G is the
293 same as that used by HL. It is surprising because the model atmosphere is expected to be more sensitive
294 to the changes in the radiative damping as G becomes smaller and smaller. Note that when our control
295 runs adopt the black radiative damping profile shown in FIG. 1a the simulated QBO periods are not
296 sensitive to the imposed semiannual forcing provided that G does not exceed the values employed by
297 HL. Similarly, when our experimental runs adopt the red radiative damping profile above 24 km shown
298 in FIG. 1a the simulated QBO periods are also not sensitive to the imposed semiannual forcing provided
299 that G does not exceed 50% of the values adopted in HL. The question naturally arises: what is
300 responsible for this unexpected behavior?

301 In Section 2, the simulated QBO periods are equal to 30 and 34.3 months when we adopted the no-
302 slip and stress-free upper boundary condition respectively with all other parameters being identical to
303 those used by HL. The results implicate the upper boundary conditions in the inconsistency. Plumb (1977)
304 pointed out that the upper boundary in HL was undesirably low and implied that raising the lid to an
305 additional 50% would be adequate for the robustness in his model. Here, we carry out a series of
306 sensitivity tests by raising the model lid gradually from 35 km to 55 km with the one-kilometer increment.
307 we will demonstrate how the behavior of the HL model with $G = 0$ converges with that of the Plumb

308 model. The modified HL model, i.e., the HL model with $G = 0$ is identical to the Plumb model except
309 that the former has the no-slip upper boundary condition while the latter has the stress-free upper
310 boundary condition. Both models share the same governing equation (5). Note that we set the radiative
311 damping rate above the 35 km level to its value at the 35 km level shown in FIG. 1a.

312 For the radiative damping profile corresponding to the reference CO₂, FIG. 6 shows that when the
313 model lid is placed at the 35 km level the simulated QBO period of 30.0 months with the no-slip upper
314 boundary condition (solid black line) is apparently shorter than that of 37.5 months with the stress-free
315 upper boundary condition (dashed black line). FIG. 6 also shows that as the model lid is raised
316 incrementally from the 35 km level to the 46 km level, the discrepancies between the simulated QBO
317 periods due to the different upper boundary conditions decrease monotonically. No matter whether we
318 adopt the no-slip or stress-free upper boundary condition, the simulated QBO period is 32.4 months for
319 the reference radiative damping profile provided that the model top is at or above the 46 km level.

320 Similarly, for the radiative damping profile corresponding to the doubled CO₂, FIG. 6 demonstrates
321 that when the model lid is placed at the 35 km level the simulated QBO period of 28.6 months with the
322 no-slip upper boundary condition (solid red line) is obviously shorter than that of 31.6 months with the
323 stress-free upper boundary condition (dashed red line). FIG. 6 also exhibits that as the model lid is raised
324 gradually from the 35 km level to the 40 km level, the discrepancies between the simulated QBO periods
325 due to the different upper boundary conditions decrease monotonically. No matter whether we adopt the
326 no-slip or stress-free upper boundary condition, the simulated QBO period for the enhanced infrared
327 cooling due to the doubled CO₂ is 30.0 months provided that the model top is at or above the 40 km level.
328 It is apparent that the required model top is lower when the radiative damping is augmented due to the
329 doubling of CO₂ because the planetary waves dissipate more steeply with height in presence of the
330 enhanced infrared cooling rates.

331 FIG. 6 suggests that when the model lid is sufficiently high the QBO period in response to the
 332 enhanced radiative damping due to the increasing CO₂ will decrease from 32.4 to 30.0 months. This
 333 7.4% decrease in the QBO period is independent of the upper boundary condition. Plass (1956) indicated
 334 that the probable error of the cooling rate was about 10% below 20 km, increasing to 30% at 50 km and
 335 that the relative differences between the cooling rates should be considerably more accurate than their
 336 magnitude. In other words, the relative differences between the various cooling rates calculated by Plass
 337 (1956) should be considerably smaller 30%. Using the HL model with its top at the 48 km level, we
 338 further conducted two experiments by adopting $G = 0$ in Eq. (1) and increasing the radiative damping
 339 corresponding to the doubled CO₂ between 30 km and 48 km by $30\% - 30\% * 30\% = 21\%$ and
 340 $30\% + 30\% * 30\% = 39\%$ respectively relative to that in the control run. The simulated QBO periods
 341 are 30.8 and 29.3 months respectively. Therefore, when the model lid is sufficiently high the QBO period
 342 in response to the enhanced radiative damping due to the doubled CO₂ will decrease by approximately
 343 $7.4\% \pm 2.5\%$.

344 Jonsson et al. (2004) showed that the doubled CO₂ induces a substantial cooling throughout most of
 345 the middle atmosphere, which in turn increases the ozone mixing ratio by 15–20% in the upper
 346 stratosphere and by 10–15% in the lower mesosphere (refer to their Figure 6). Incorporating this increase
 347 into the ozone profile for the doubled CO₂, we recalculated the ratio of α_2 , the Newtonian cooling
 348 coefficient for the doubled CO₂, to α_1 , the Newtonian cooling coefficient for the reference CO₂. Our
 349 calculated α_2/α_1 is only slightly increased as compared with that shown FIG. 1b no matter whether the
 350 CO₂ absorption band is $5\ \mu\text{m} - 100\ \mu\text{m}$ or $12\ \mu\text{m} - 18\ \mu\text{m}$ (figure not shown). It is not unexpected
 351 because the infrared radiative cooling by ozone is significantly smaller than that by CO₂ (refer to Fig. 1
 352 in Dickinson 1973) and, as a result, the 15–20% increases in the ozone mixing ratio will not make a

noticeable difference. Consequently, the QBO period is expected to be marginally influenced by the change in the radiative damping due to the increase in ozone in response to the doubled CO₂.

Note that N , the Brunt-Väisälä frequency, in Eqs. (2) and (3) also changes with increasing CO₂. Richter et al. (2020b) showed that N^2 would be decreased by $\sim 5\%$ in the stratosphere when CO₂ is doubled (refer to their Figure 2c). We used the HL model to conduct a sensitivity test by adopting $G = 0$ in Eq. (1) with the radiative damping profile corresponding to the doubled CO₂ and the top of the models at the 48 km level. The rest of parameters in this sensitivity test are identical to those in all the previous runs except that the Brunt-Väisälä frequency in this experimental run was 2.5% smaller than that in the control run. The models were run for 1000 years to further increase the spectral resolution. We found that when the Brunt-Väisälä frequency was decreased by 2.5%, the simulated QBO period was slightly lengthened from 30 months to 30.2 months (figure not shown). In other words, the impact of decreasing stratospheric buoyancy frequency on the QBO period is almost negligible.

Analyzing eleven CCMI-1 REF-C2 climate–chemistry simulations, Eichinger and Šácha (2020) showed that the scale height in the stratosphere decreases by 2.3% per century. Accordingly, we used the HL model to conduct another sensitivity test by adopting $G = 0$ in Eq. (1) with the radiative damping profile corresponding to the doubled CO₂ and the top of the models at the 48 km level. The rest of parameters in this sensitivity test are identical to those in all the previous control runs except that the scale height in this experimental run was 2.3% smaller than that in the control run. The model was also run for 1000 years for the sake of higher spectral resolution. We found that when the scale height was decreased by 2.3%, the simulated QBO period was also shortened by about 2.3%, i.e., from 30 months to 29.3 months (figure not shown). Apparently, the shortening of the QBO period due to the warming climate is ascribed less to the shrinkage of the scale height in the stratosphere than to the enhancing of

375 the stratospheric radiative damping. Together, the shrinking scale height and the increasing radiative
376 damping shorten the QBO period by about 9.6%.

377

378 **5. Conclusions**

379 Plumb (1977) envisioned that stratospheric climate change would give rise to long-term changes in
380 the QBO period due to changes in radiative damping and the Brunt-Väisälä frequency. Using one-
381 dimensional (1D) models and taking into account the uncertainty due to the radiative damping rate, we
382 found that the enhanced radiative damping arising from the doubling of CO₂ leads to the shortening of
383 the QBO period by about $7.4\% \pm 2.5\%$ provided that the model top is higher than the 46 km level.
384 Furthermore, when we incorporated both the 2.3% shrinkage of the scale height and the enhanced
385 radiative damping, the QBO period is shortened by about 9.6%. In addition, the impact of decreasing
386 stratospheric buoyancy frequency and increasing radiative damping due to the increased ozone on the
387 QBO period is marginal. Note that those models include neither gravity waves nor tropical upwelling
388 and assume that there are no changes in wave fluxes entering the equatorial stratosphere.

389 From a comprehensive model perspective, Richter et al. (2020b) showed that the changes in period
390 of the QBO in warming climate simulations varied quite significantly among these models. Some models
391 projected longer mean periods and some shorter mean periods for the QBO in a future warmer climate.
392 They argue that uncertainty in the representation of the parameterized gravity waves is the most likely
393 cause of the spread among the QBOi models in the QBO's response to climate change.

394 In addition, CO₂ increases in the NASA Goddard Institute for Space Studies Model E2.2-AP (Rind
395 et al. 2020; Orbe et al. 2020) lead to a decrease of both QBO period and QBO amplitude (DallaSanta et
396 al., 2021). The period decrease is associated with increases in lower stratospheric momentum fluxes
397 (related to parameterized convection), a finding consistent with Geller et al. (2016a, 2016b) and Richter

398 et al. (2020b). The amplitude decrease is associated with a strengthened residual mean circulation, also
399 consistent with the literature, although the vertical structure of the circulation response is nontrivial. It
400 is worth mentioning that horizontal momentum flux divergences could also play an important role in
401 weakening the QBO (Match and Fueglistaler, 2019, 2020).

402 Our 1D models only explored how the QBO period responds to the enhancing radiative damping of
403 planetary waves, the shrinking scale height in the stratosphere, and the decreasing stratospheric
404 buoyancy frequency due to the increasing CO₂ concentration. In order to investigate how those factors
405 affect gravity waves which play an even more important role in determining the QBO period than
406 planetary waves, high-resolution models such as those used by Kawatani et al. (2011, 2019) are desirable
407 to further our understanding. Ultimately, how the QBO period changes in response to the increasing CO₂
408 will be determined by the combined effects of the strengthening of tropical upwelling, the increasing of
409 wave fluxes entering the equatorial stratosphere, the enhancing of radiative damping, and the shrinking
410 of the scale height in the stratosphere, which warrants further research.

411

412 **Data availability**

413 Any data used in this paper can be made available from the corresponding author upon request.

414

415 **Author contributions**

416 All authors made equal contributions to this work.

417

418 **Competing interests**

419 The authors declare that they have no conflict of interest.

420

421 **Acknowledgements:** Climate modeling at GISS is supported by the NASA Modeling, Analysis and
422 Prediction program, and resources supporting this work were provided by the NASA High-End
423 Computing (HEC) Program through the NASA Center for Climate Simulation (NCCS) at Goddard Space
424 Flight Center. KD acknowledges support from the NASA Postdoctoral Program. The authors thank the
425 editor Peter Haynes and two anonymous reviewers for their helpful comments, which led to an improved
426 paper. The authors also acknowledge very useful discussions with Drs. Geller and Orbe.

427

428 **References**

- 429 Andrews, D. G., Holton, J. R., and Leovy, C. B.: Middle Atmosphere Dynamics, Academic Press, 489
430 pp, 1987.
- 431 Baldwin, M. P., Gray, L. J., Dunkerton, T. J., Hamilton, K., Haynes, P. H., Randel, W. J., Holton, J. R.,
432 Alexander, M. J., Hirota, I., Horinouchi, T., Jones, D. B. A., Kinnnersley, J. S., Marquardt, C., Sato,
433 K., and Takahashi, M.: The Quasi-biennial oscillation, *Rev. Geophys.*, 39, 179–229,
434 <https://doi.org/10.1029/1999RG000073>, 2001.
- 435 Berk, A., Anderson, G. P., Acharya, P. K., Shettle, E. P.: MODTRAN5 version 2 user’s manual, Spectral
436 Sciences, Inc., Burlington MA and Air force Geophysics Laboratory, Hanscom AFB, MA, 2008.
- 437 Butchart, N.: The Brewer-Dobson circulation, *Rev. Geophys.*, 52, 157–
438 184, <https://doi.org/10.1002/2013RG000448>, 2014.
- 439 Butchart, N., Scaife, A. A., Bourqui, M., Grandpré, J., Hare, S. H., Kettleborough, J., Langematz, U.,
440 Manzini, E., Sassi, F., Shibata, K., Shindell, D. and Sigmond, M.: Simulations of anthropogenic
441 change in the strength of the Brewer–Dobson circulation, *Climate Dynamics*, 27, 727–741,
442 <https://doi.org/10.1007/s00382-006-0162-4>, 2006.

443 Butchart, N., Anstey, J., Hamilton, K., Osprey, S., McLandress, C., Bushell, A. C., Kawatani, Y., Kim,
 444 Y.-H., Lott, F., Scinocca, J., Stockdale, T.N., Andrews, M., Bellprat, O., Braesicke, P., Cagnazzo,
 445 C., Chen, C.-C., Chun, H.-Y., Dobrynin, M., Garcia, R., Garcia-Serrano, J., Gray, L.J., Holt, L.,
 446 Kerzenmacher, T., Naoe, H., Pohlmann, H., Richter, J. H., Scaife, A.A., Schenzinger, V., Serva, F.,
 447 Versick, S., Watanabe, S., Yoshida, K. and Yukimoto, S.: Overview of experiment design and
 448 comparison of models participating in phase 1 of the SPARC Quasi-Biennial Oscillation initiative
 449 (QBOi), *Geoscientific Model Development*, 11, 1009–1032. [https://doi.org/10.5194/gmd-11-1009-](https://doi.org/10.5194/gmd-11-1009-2018)
 450 [2018](https://doi.org/10.5194/gmd-11-1009-2018), 2018.

451 Butchart, N., Anstey, J. A., Kawatani, Y., Osprey, S. M., Richter, J. H., Wu, T.: QBO changes in CMIP6
 452 climate projections, *Geophys. Res. Lett.*, 47, 1–10. <https://doi.org/10.1029/2019GL086903>, 2020.

453 Camargo, S. J. and Sobel, A. H.: Revisiting the influence of the quasi-biennial oscillation on tropical
 454 cyclone activity, *J. Climate*, 23, 5810–5825, <https://doi.org/10.1175%2F2010JCLI3575.1>, 2010.

455 Collimore, C. C., Martin, D. W., Hitchman, M. H., Huesmann, A., and Waliser, D. E.: On the
 456 relationship between the QBO and tropical deep convection, *J. Climate*, 16, 2552–2568,
 457 [https://doi.org/10.1175/1520-0442\(2003\)016%3C2552:OTRBTQ%3E2.0.CO;2](https://doi.org/10.1175/1520-0442(2003)016%3C2552:OTRBTQ%3E2.0.CO;2), 2003.

458 DallaSanta, K., Orbe, C., Rind, D., Nazarenko, L., and Jonas, J.: Dynamical and trace gas responses of
 459 the Quasi-Biennial Oscillation to increased CO₂, *J. Geophys. Res. Atmos.*, 126, e2020JD034151.
 460 <https://doi.org/10.1029/2020JD034151>, 2021.

461 Dickinson, R. E.: Method of parameterization for infrared cooling between altitudes of 30 and 70
 462 kilometers, *J. Geophys. Res.*, 78, 4451–4457, <https://doi.org/10.1029/JC078i021p04451>, 1973.

463 Dunkerton, T. J.: The role of gravity waves in the quasi-biennial oscillation, *J. Geophys. Res.*, 102,
 464 26053–26076, <https://doi.org/10.1029/96JD02999>, 1997.

465 Ebdon, R. A.: Notes on the wind flow at 50 mb in tropical and subtropical regions in January 1957 and
 466 in 1958, Q. J. Roy. Meteor. Soc., 86, 540–542, <https://doi.org/10.1002/qj.49708637011>, 1960.

467 Eichinger, R. and Šácha, P.: Overestimated acceleration of the advective Brewer-Dobson circulation due
 468 to stratospheric cooling, Q. J. R. Meteorol. Soc., 1-15, <https://doi.org/10.1002/qj.3876>, 2020.

469 Fels, S. B.: A parameterization of scale-dependent radiative damping rates in the middle atmosphere, J.
 470 Atmos. Sci., 39, 1141–1152, [https://doi.org/10.1175/1520-0469\(1982\)039%3C1141:APOSDR%3E2.0.CO;2](https://doi.org/10.1175/1520-0469(1982)039%3C1141:APOSDR%3E2.0.CO;2), 1982.

472 Fels, S. B.: Radiative-dynamical interactions in the middle atmosphere, Advances in Geophysics, Vol.
 473 28A, Academic Press, 277–300, [https://doi.org/10.1016/S0065-2687\(08\)60227-7](https://doi.org/10.1016/S0065-2687(08)60227-7), 1985.

474 Garfinkel, C. I. and Hartmann, D. L.: The influence of the quasi-biennial oscillation on the troposphere
 475 in winter in a hierarchy of models. Part I: Simplified dry GCMs, J. Atmos. Sci., 68, 1273–1289,
 476 <https://doi.org/10.1175%2F2011JAS3665.1>, 2011a.

477 Garfinkel, C. I. and Hartmann, D. L.: The influence of the quasi-biennial oscillation on the troposphere
 478 in winter in a hierarchy of models. Part II: Perpetual winter WACCM runs, J. Atmos. Sci., 68, 2026–
 479 2041, <https://doi.org/10.1175%2F2011JAS3702.1>, 2011b.

480 Geller, M. A., Zhou, T., Shindell, D., Ruedy, R., Aleinov, I., Nazarenko, L., Tausnev, N. L., Kelley, M.,
 481 Sun, S., Cheng, Y., Field, R. D., and Faluvegi, G.: Modeling the QBO-improvements resulting from
 482 higher-model vertical resolution, J. Adv. Model. Earth Syst., 8, 1092–1105,
 483 <https://doi.org/10.1002/2016MS000699>, 2016a.

484 Geller, M. A., Zhou, T., and Yuan, W.: The QBO, gravity waves forced by tropical convection, and
 485 ENSO, J. Geophys. Res. Atmos., 121, 8886–8895, <https://doi.org/10.1002/2015JD024125>, 2016b.

486 Gidden, M. J., Riahi, K., Smith, S. J., Fujimori, S., Luderer, G., Kriegler, E., van Vuuren, D. P., van den
 487 Berg, M., Feng, L., Klein, D., Calvin, K., Doelman, J. C., Frank, S., Fricko, O., Harmsen, M.,

488 Hasegawa, T., Havlik, P., Hilaire, J., Hoesly, R., Horing, J., Popp, A., Stehfest, E., and Takahashi,
 489 K.: Global emissions pathways under different socioeconomic scenarios for use in CMIP6: a dataset
 490 of harmonized emissions trajectories through the end of the century, *Geosci. Model Dev.*, 12, 1443–
 491 1475, <https://doi.org/10.5194/gmd-12-1443-2019>, 2019.

492 Giorgetta, M. A. and Doege, M. C.: Sensitivity of the Quasi-Biennial Oscillation to CO₂ doubling,
 493 *Geophys. Res. Lett.*, 32, L08701. <https://doi.org/10.1029/2004GL021971>, 2005.

494 Giorgetta, M. A., Bengtson, L., and Arpe, K.: An investigation of QBO signals in the east Asian and
 495 Indian monsoon in GCM experiments, *Climate Dynamics*, 15, 435–450,
 496 <https://doi.org/10.1007/s003820050292>, 1999.

497 Giorgetta, M. A., Manzini, E., and Roeckner, E.: Forcing of the quasi-biennial oscillation from a broad
 498 spectrum of atmospheric waves, *Geophys. Res. Lett.*, 29, <https://doi.org/10.1029/2002GL014756>,
 499 2002.

500 Giorgetta, M. A., Manzini, E., and Roeckner, E., Esch, M., and Bengtsson, L.: Climatology and forcing
 501 of the quasi-biennial oscillation in the MAECHM5 model, *J. Climate*, 19, 3882–3901,
 502 <https://doi.org/10.1175/JCLI3830.1>, 2006.

503 Gray, W. M.: Atlantic seasonal hurricane frequency. Part I: El Niño and 30-mb quasi-biennial oscillation
 504 influences, *Mon. Wea. Rev.*, 112, 1649–1688, [https://doi.org/10.1175/1520-0493\(1984\)112%3C1649:ASHFPI%3E2.0.CO;2](https://doi.org/10.1175/1520-0493(1984)112%3C1649:ASHFPI%3E2.0.CO;2), 1984.

506 Gray, W. M., Sheaffer, J. D., and Knaff, J.: Influence of the stratospheric QBO on ENSO variability, *J.*
 507 *Meteor. Soc. Jpn.*, 70, 975–995, https://doi.org/10.2151/jmsj1965.70.5_975, 1992.

508 Hamilton, K.: The vertical structure of the quasi-biennial oscillation: Observations and theory, *Atmos.*
 509 *Ocean*, 19, 236–250, <http://dx.doi.org/10.1080/07055900.1981.9649111>, 1981.

510 Hansen, F., Matthes, K., and Wahl, S.: Tropospheric QBO–ENSO interactions and differences between
 511 the Atlantic and Pacific, *J. Climate*, 29, 1353–1368, <https://doi.org/10.1175/JCLI-D-15-0164.1>,
 512 2016

513 Hasebe, F.: Quasi-biennial oscillations of ozone and diabatic circulation in the equatorial stratosphere, *J.*
 514 *Atmos. Sci.*, 51, 729–745, [https://doi.org/10.1175/1520-0469\(1994\)051%3c0729:QBOOOA%3e2.0.CO;2](https://doi.org/10.1175/1520-0469(1994)051%3c0729:QBOOOA%3e2.0.CO;2), 1994.

516 Hitchman, M. H., and Huesmann, A. S.: Seasonal influence of the quasi-biennial oscillation on
 517 stratospheric jets and Rossby wave breaking, *J. Atmos. Sci.*, 66, 935–946,
 518 <https://doi.org/10.1175%2F2008JAS2631.1>, 2009.

519 Ho, C.-H., Kim, H.-S., Jeong, J.-H., and Son, S.-W.: Influence of stratospheric quasi-biennial oscillation
 520 on tropical cyclone tracks in the western North Pacific, *Geophys. Res. Lett.*, 36, L06702,
 521 <http://dx.doi.org/10.1029/2009GL037163>, 2009.

522 Holt, L., Lott, F., Garcia, R., Kiladis, G.N., Anstey, J.A., Braesicke, P., Bushell, A.C., Butchart, N.,
 523 Cagnazzo, C., Chen, C.-C., Chun, H.-Y., Hamilton, K., Kawatani, Y., Kerzenmacher, T., Kim, Y.-
 524 H., McLandress, C., Naoe, H., Osprey, S., Richter, J.H., Scinocca, J., Serva, F., Versick, S.,
 525 Watanabe, S., Yoshida, K., and Yukimoto, S.: An evaluation of tropical waves and wave forcing of
 526 the QBO in the QBOi models, *Q. J. R. Meteorol. Soc.*, <https://doi.org/10.1002/qj.3827>, 2020.

527 Holton, J. R. and Lindzen, R. S.: An updated theory for the quasi-biennial cycle of the tropical
 528 stratosphere, *J. Atmos. Sci.*, 29, 1076–1080, [https://doi.org/10.1175/1520-0469\(1972\)029%3c1076:AUTFTQ%3e2.0.CO;2](https://doi.org/10.1175/1520-0469(1972)029%3c1076:AUTFTQ%3e2.0.CO;2), 1972.

530 Holton, J. R. and Tan, H.: The Influence of the equatorial quasi-biennial oscillation on the global
 531 circulation at 50 mb, *J. Atmos. Sci.*, 37, 2200–2208, [https://doi.org/10.1175/1520-0469\(1980\)037%3c2200:TIOTEQ%3e2.0.CO;2](https://doi.org/10.1175/1520-0469(1980)037%3c2200:TIOTEQ%3e2.0.CO;2), 1980.

533 Huang, B. H., Hu, Z. Z., Kinter, J. L., Wu, Z. H., and Kumar, A.: Connection of stratospheric QBO with
 534 global atmospheric general circulation and tropical SST. Part I: Methodology and composite life
 535 cycle, *Climate Dynamics*, 38, 1–23, <https://doi.org/10.1007/s00382-011-1250-7>, 2012.

536 Jin, Z., Zhang, Y.-C., Del Genio, A., Schmidt, G., and Kelley, M.: Cloud scattering impact on thermal
 537 radiative transfer and global longwave radiation, *J. Quant. Spectrosc. Radiat. Transfer*, 239, 106669,
 538 <https://doi.org/10.1016/j.jqsrt.2019.106669>, 2019.

539 Jonsson, A., de Grandpre, J., Fomichev, V., McConnell, J., and Beagley, S.: Doubled CO₂-induced
 540 cooling in the middle atmosphere: Photochemical analysis of the ozone radiative feedback, *J.*
 541 *Geophys. Res.*, 109, D24103, <https://doi.org/10.1029/2004JD005093>, 2004.

542 Kawatani, Y. and Hamilton, K.: Weakened stratospheric Quasi-Biennial Oscillation driven by increased
 543 tropical mean upwelling, *Nature*, 497, 478–481, <https://doi.org/10.1038/nature12140>, 2013.

544 Kawatani, Y., Takahashi, M., Sato, K., Alexander, S. P., and Tsuda, T.: Global distribution of
 545 atmospheric waves in the equatorial upper troposphere and lower stratosphere: AGCM simulation
 546 of sources and propagation, *J. Geophys. Res.*, 114, D01102, <https://doi.org/10.1029/2008JD010374>,
 547 2009.

548 Kawatani, Y., Watanabe, S., Sato, K., Dunkerton, T. J., Miyahara, S., and Takahashi, M.: The roles of
 549 equatorial trapped waves and internal inertia-gravity waves in driving the Quasi-Biennial oscillation.
 550 Part I: Zonal mean wave forcing, *J. Atmos. Sci.*, 67, 963–980,
 551 <https://doi.org/10.1175/2009JAS3222.1>, 2010.

552 Kawatani, Y., Hamilton, K., and Watanabe, S.: The quasi-biennial oscillation in a double CO₂ climate,
 553 *J. Atmos. Sci.*, 68, 265–283, <https://doi.org/10.1175/2010JAS3623.1>, 2011.

554 Kawatani, Y, Lee, J. N., and Hamilton, K.: Interannual variations of stratospheric water vapor in MLS
 555 observations and climate model simulations, *J. Atmos. Sci.*, 71, 4072–4085,
 556 <https://doi.org/10.1175/JAS-D-14-0164.1>, 2014.

557 Kawatani, Y., Hamilton, K., Sato, K., Dunkerton, T. J., Watanabe, S., and Kikuchi, K.: ENSO Modulation
 558 of the QBO: Results from MIROC Models with and without Nonorographic Gravity Wave
 559 Parameterization, *J. Atmos. Sci.*, 76, 3893–3917, <https://doi.org/10.1175/JAS-D-19-0163.1>, 2019.

560 Labitzke, K.: On the interannual variability of the middle stratosphere during the northern winters, *J.*
 561 *Meteorol. Soc. Jpn.*, 80, 963–971, http://doi.org/10.2151/jmsj1965.60.1_124, 1982.

562 Lait, L. R., Schoeberl, M. R., and Newman, P. A.: Quasi-biennial modulation of the Antarctic ozone
 563 depletion, *J. Geophys. Res.*, 94, 11559–11571, <http://dx.doi.org/10.1029/JD094iD09p11559>, 1989.

564 Li, F., Austin, J., and Wilson, R. J.: The strength of the Brewer–Dobson circulation in a changing climate:
 565 Coupled chemistry–climate model simulations, *J. Climate*, 21, 40–57,
 566 <https://doi.org/10.1175/2007JCLI1663.1>, 2008.

567 Liess, S. and Geller, M. A.: On the relationship between QBO and distribution of tropical deep
 568 convection, *J. Geophys. Res.*, 117, D03108, <http://dx.doi.org/10.1029/2011JD016317>, 2012.

569 Lindzen, R. S.: Equatorial planetary waves in shear: Part I, *J. Atmos. Sci.* 28, 609–622,
 570 [https://doi.org/10.1175/1520-0469\(1971\)028%3C0609:EPWISP%3E2.0.CO;2](https://doi.org/10.1175/1520-0469(1971)028%3C0609:EPWISP%3E2.0.CO;2), 1971.

571 Lindzen, R. S. and Holton, J. R.: A theory of the quasi-biennial oscillation, *J. Atmos. Sci.*, 25, 1095–
 572 1107, [https://doi.org/10.1175/1520-0469\(1968\)025%3C1095:ATOTQB%3E2.0.CO;2](https://doi.org/10.1175/1520-0469(1968)025%3C1095:ATOTQB%3E2.0.CO;2), 1968.

573 Manabe, S. and Wetherald, R. T.: Thermal equilibrium of the atmosphere with a given distribution of
 574 relative humidity, *J. Atmos. Sci.*, 24, 241–259, [https://doi.org/10.1175/1520-0469\(1967\)024%3C0241:TEOTAW%3E2.0.CO;2](https://doi.org/10.1175/1520-0469(1967)024%3C0241:TEOTAW%3E2.0.CO;2), 1967.

576 Marshall, A. G. and Scaife, A. A.: Impact of the QBO on surface winter climate, *J. Geophys. Res.*, 114,
577 D18110, <http://dx.doi.org/10.1029/2009JD011737>, 2009.

578 Match, A., and Fueglistaler, S.: The buffer zone of the quasi-biennial oscillation, *J. Atmos. Sci.*, 76, 3553–
579 3567, <https://doi.org/10.1175/JAS-D-19-0151.1>, 2019

580 Match, A., and Fueglistaler, S.: Mean-flow damping forms the buffer zone of the quasi-biennial
581 oscillation: 1D theory. *J. Atmos. Sci.*, 77, 1955–1967, <https://doi.org/10.1175/JAS-D-19-0293.1>,
582 2020.

583 Matsuno, T.: Numerical integrations of primitive equations by use of a simulated backward difference
584 method, *J. Meteor. Soc. Japan*, 44, 76–84, https://doi.org/10.2151/jmsj1965.44.1_76, 1966.

585 Orbe, C., Rind, D., Jonas, J., Nazarenko, L., Faluvegi, G., Murray, L.T., Shindell, D.T., Tsigaridis, K.,
586 Zhou, T., Kelley, M., and Schmidt, G.: GISS Model E2.2: A climate model optimized for the middle
587 atmosphere. Part 2: Validation of large-scale transport and evaluation of climate response. *J.*
588 *Geophys. Res. Atmos.*, 125, e2020JD033151, <https://doi.org/10.1029/2020JD033151>, 2020.

589 Plass, G. N.: The influence of the 15 μ carbon-dioxide band on the atmospheric infra-red cooling rate,
590 *Quart. J. Roy. Meteor. Soc.*, 82, 310–324, <https://doi.org/10.1002/qj.49708235307>, 1956.

591 Plumb, R. A.: The interaction of two internal waves with the mean flow: Implications for the theory of
592 the quasi-biennial oscillation, *J. Atmos. Sci.*, 34, 1847–1858, [https://doi.org/10.1175/1520-0469\(1977\)034<1847:TIOTIW>2.0.CO;2](https://doi.org/10.1175/1520-0469(1977)034<1847:TIOTIW>2.0.CO;2), 1977.

594 Reed, R. J., Campbell, W. J., Rasmussen, L. A., and Rogers, D. G.: Evidence of a downward-propagating,
595 annual wind reversal in the equatorial stratosphere, *J. Geophys. Res.*, 66, 813–818,
596 <http://dx.doi.org/10.1029/JZ066i003p00813>, 1961.

597 Richter, J. H., Anstey, J. A., Butchart, N., Kawatani, Y., Meehl, G. A., Osprey, S., & Simpson, I. R.,
 598 2020b: Progress in simulating the quasi-biennial oscillation in CMIP models. *Journal Geophysical*
 599 *Research: Atmospheres*, 125, e2019JD032362, <https://doi.org/10.1029/2019JD032362>, 2020a.

600 Richter, J. H., Butchart, N., Kawatani, Y., Bushell, A. C., Holt, L., Serva, F., Anstey, J., Simpson, I. R.,
 601 Osprey, S., Hamilton, K., Braesicke, P., Cagnazzo, C., Chen, C.-C., Garcia, R. R., Gray, L. J.,
 602 Kerzenmacher, T., Lott, F., McLandress, C., Naoe, H., Scinocca, J., Stockdale, T. N., Versick, S.,
 603 Watanabe, S., Yoshida, K., Yukimoto, S.: Response of the Quasi-Biennial Oscillation to a warming
 604 climate in global climate models, *Q. J. R. Meteorol. Soc.*, 1–29. <https://doi.org/10.1002/qj.3749>,
 605 2020b.

606 Rind, D., Jonas, J., Balachandran, N., Schmidt, G., and Lean, J.: The QBO in two GISS global climate
 607 models: 1. Generation of the QBO, *J. Geophys. Res. Atmos.*, 119, 8798–8824,
 608 <https://doi.org/10.1002/2014JD021678>, 2014.

609 Rind, D., Orbe, C., Jonas, J., Nazarenko, L., Zhou, T., Kelley, M., Lacis, A., Shindell, D., Faluvegi,
 610 Russell, G., Bauer, M., Schmidt, G., Romanou, A., and Tausnev, N.: GISS Model E2.2: A climate
 611 model optimized for the middle atmosphere — Model structure, climatology, variability and climate
 612 sensitivity, *J. Geophys. Res. Atmos.*, 125, e2019JD032204, <https://doi.org/10.1029/2019JD032204>,
 613 2020.

614 Saravanan, R.: A multiwave model of the quasi-biennial oscillation, *J. Atmos. Sci.*, 47, 2465–2474,
 615 [https://doi.org/10.1175/1520-0469\(1990\)047%3C2465:AMMOTQ%3E2.0.CO;2](https://doi.org/10.1175/1520-0469(1990)047%3C2465:AMMOTQ%3E2.0.CO;2), 1990.

616 Scaife, A. A., Butchart, N., Warner, C. D., Stainforth, D., Norton, W., and Austin, J.: Realistic quasi-
 617 biennial oscillations in a simulation of the global climate, *Geophys. Res. Lett.*, 27, 3481–3484,
 618 <https://doi.org/10.1029/2000GL011625>, 2000.

619 Schirber, S., Manzini, E., Krismer, T. and Giorgetta, M.: The Quasi-Biennial Oscillation in a warmer
 620 climate: sensitivity to different gravity wave parameterizations, *Climate Dynamics*, 45, 825–
 621 836, <https://doi.org/10.1007/s00382-014-2314-2>, 2015.

622 Trepte, C. R. and Hitchman, M. H.: Tropical stratospheric circulation deduced from satellite aerosol data,
 623 *Nature*, 355, 626–628, <https://doi.org/10.1038/355626a0>, 1992.

624 Watanabe, S. and Kawatani, Y.: Sensitivity of the QBO to mean tropical upwelling under a changing
 625 climate simulated with an Earth System Model, *Journal of the Meteorological Society of Japan*,
 626 Series II, 90A, 351–360, <https://doi.org/10.2151/jmsj.2012-A20>, 2012.

627 Yoo, C. and Son, S.-W.: Modulation of the boreal wintertime Madden-Julian oscillation by the
 628 stratospheric quasi-biennial oscillation, *Geophys. Res. Lett.*, 43, 1392–1398,
 629 <https://doi.org/10.1002/2016GL067762>, 2016.

630 Zawodny, J. M. and McCormick, M. P.: Stratospheric Aerosol and Gas Experiment II measurements of
 631 the quasi-biennial oscillations in ozone and nitrogen dioxide, *J. Geophys. Res.*, 96, 9371– 9377,
 632 <http://dx.doi.org/10.1029/91JD00517>, 1991.

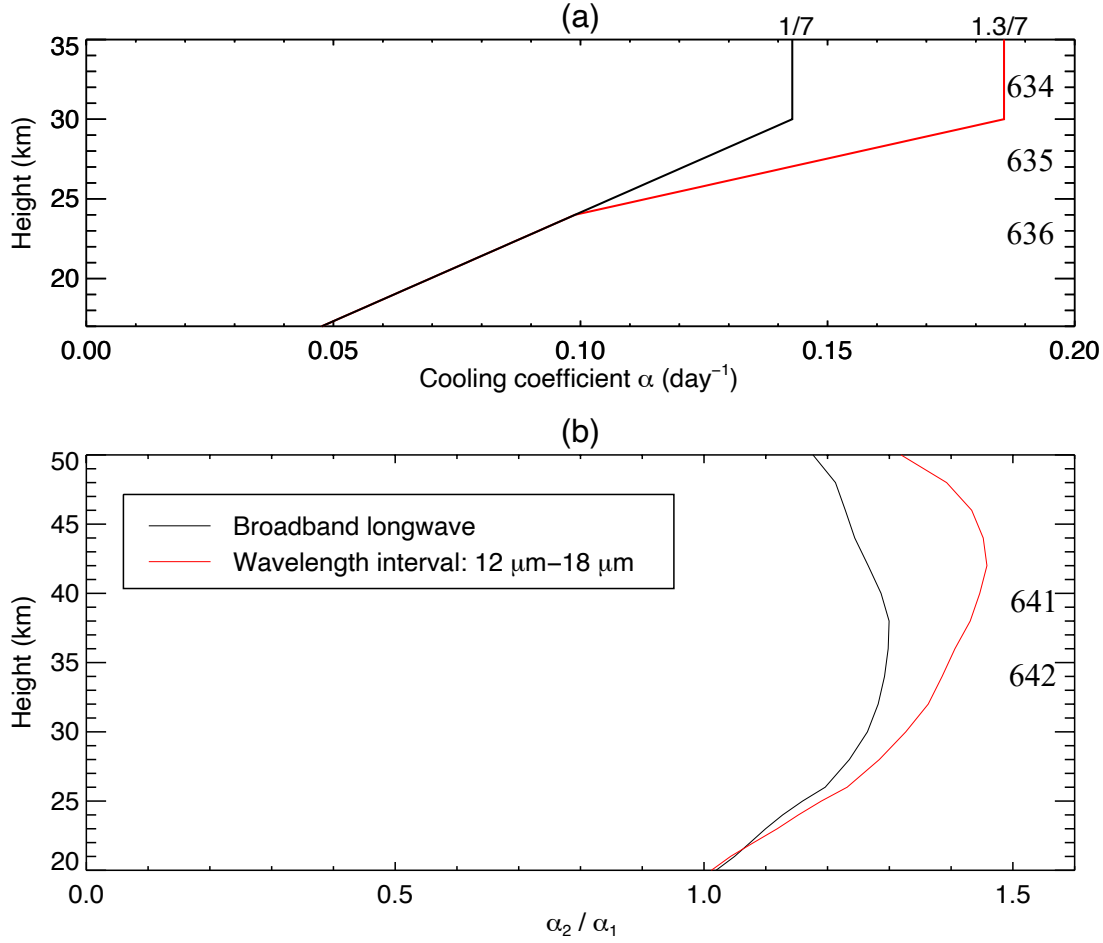


FIG. 1: (a) Profiles of Newtonian cooling coefficients: The smaller values (black line) are used for the control runs while the larger values (red line) are used for the experimental runs. (b) Profiles of the ratio of α_2 to α_1 , where α_1 and α_2 denote the Newtonian cooling coefficient for the reference CO₂ and the doubled CO₂, respectively. The black line depicts the ratio for the broadband longwave (5 μm – 100 μm) and the red line delineates that for the CO₂ absorption band (12 μm – 18 μm).

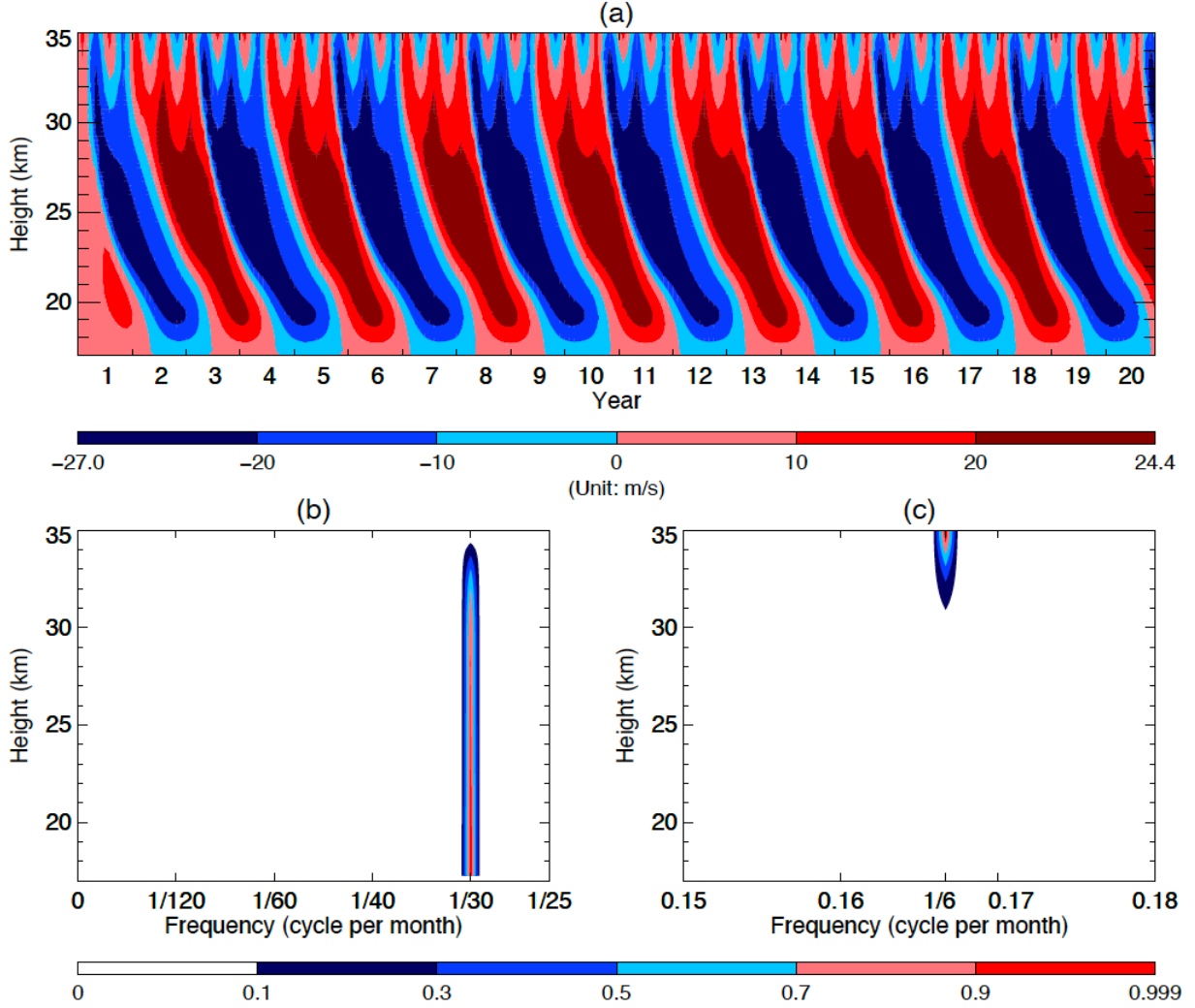


FIG. 2: (a) Time–height section of the monthly averaged mean zonal wind over the first 20 years from the HL’s original model. (b) and (c) Frequency–height section of the power spectral densities (PSD) of the standardized monthly averaged mean zonal wind of the 100 years. Note that in order to better visualize the PSD in (b) and (c), we trimmed off the blank segments for the frequencies ranging from $\frac{1}{25}$ to 0.15 cycle per month and those ranging from 0.18 to 0.5 cycle per month.

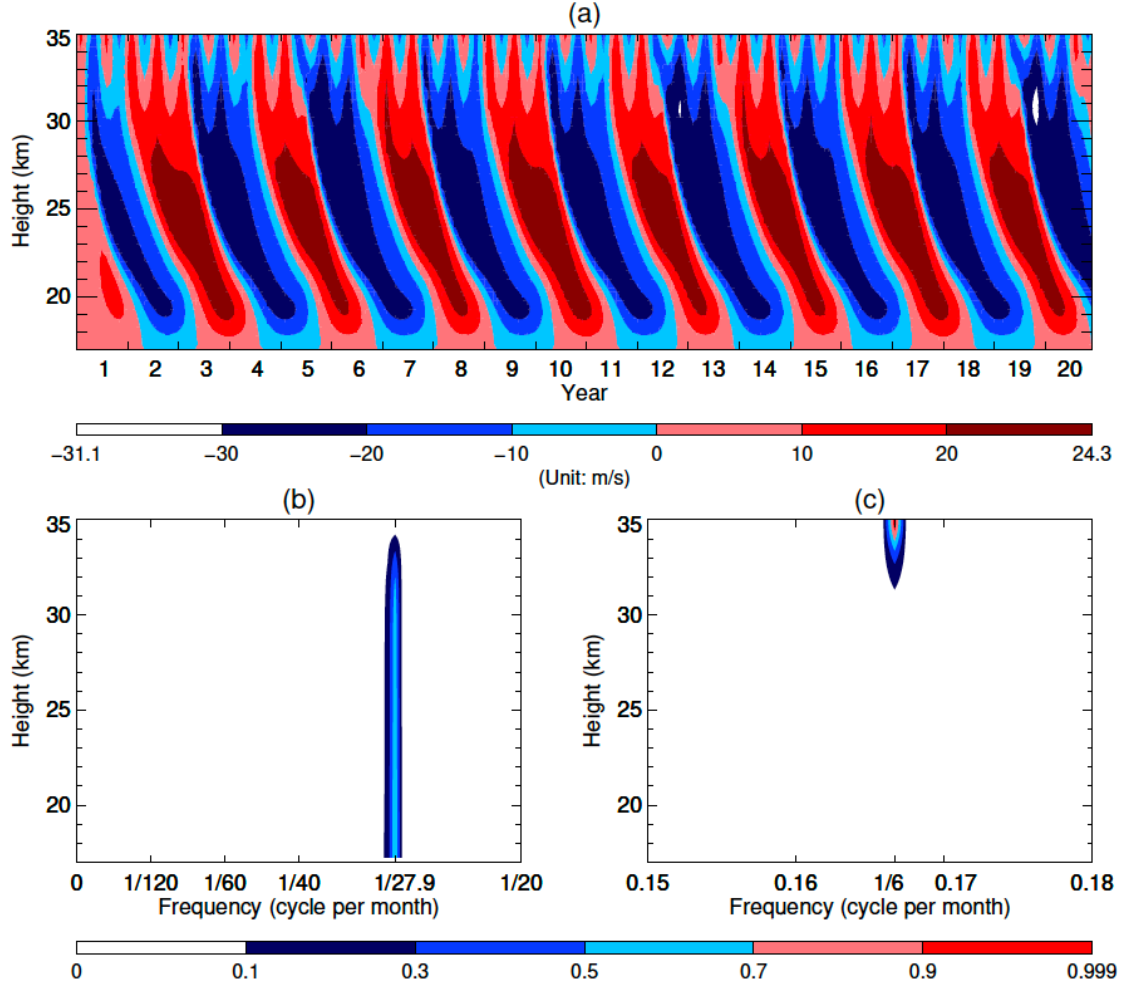


FIG. 3: (a) Same as FIG. 2a, but with the enhanced $\alpha(z)$ depicted as the red line in FIG. 1a. (b) and (c) Frequency–height section of the power spectral densities (PSD) of the standardized monthly averaged mean zonal wind of the 100 years. Note that in order to better visualize the PSD in (b) and (c), we trimmed off the blank segments for the frequencies ranging from $\frac{1}{20}$ to 0.15 cycle per month and those ranging from 0.18 to 0.5 cycle per month.

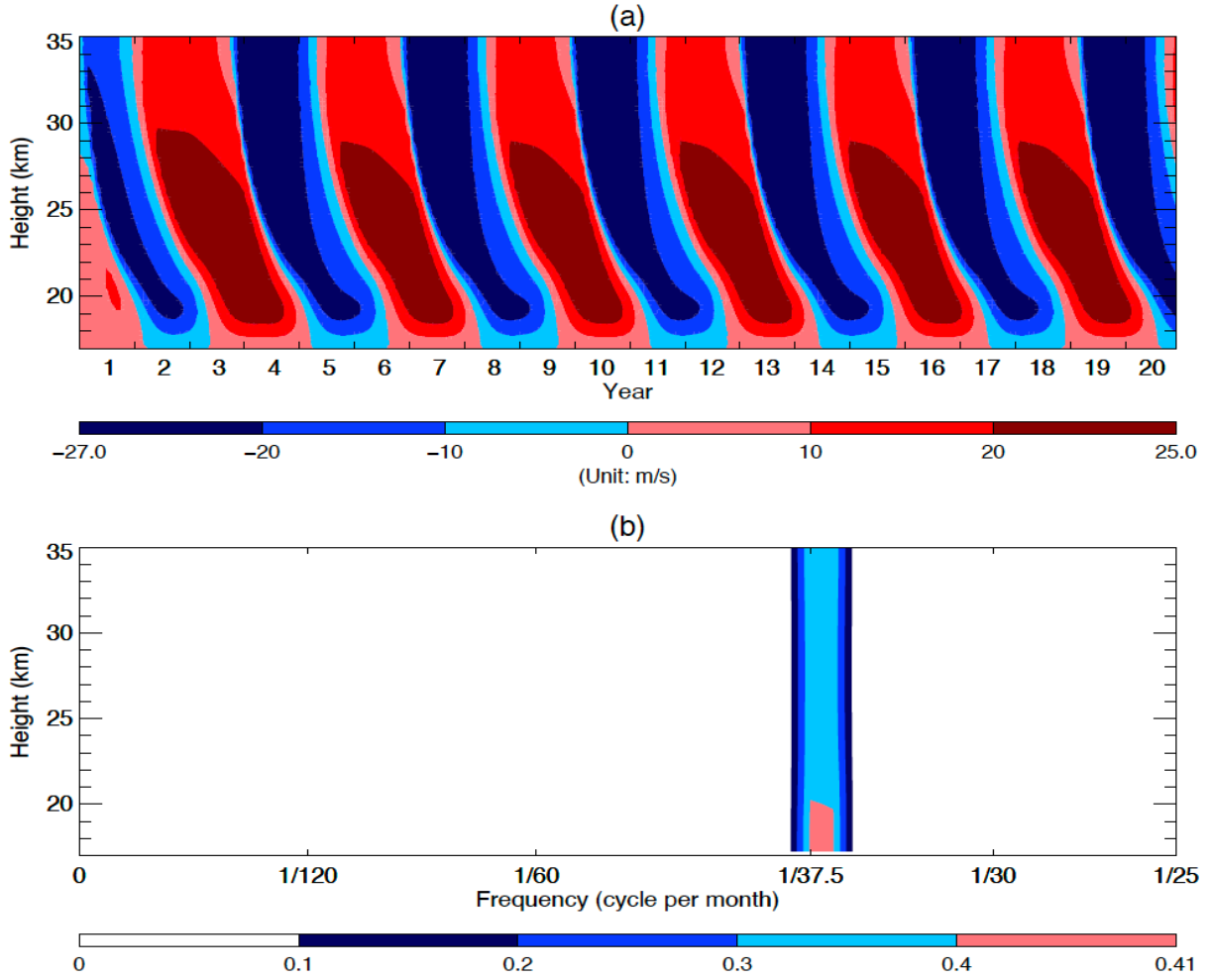


FIG. 4: (a) Time–height section of the monthly averaged mean zonal wind over the first 20 years from the HL’s model without the semiannual forcing. (b) Frequency–height section of the power spectral densities (PSD) of the standardized monthly averaged mean zonal wind of the 100 years. Note that in order to visualize the PSD, we trimmed off the blank segment for the frequencies ranging from $\frac{1}{25}$ to 0.5 cycle per month.

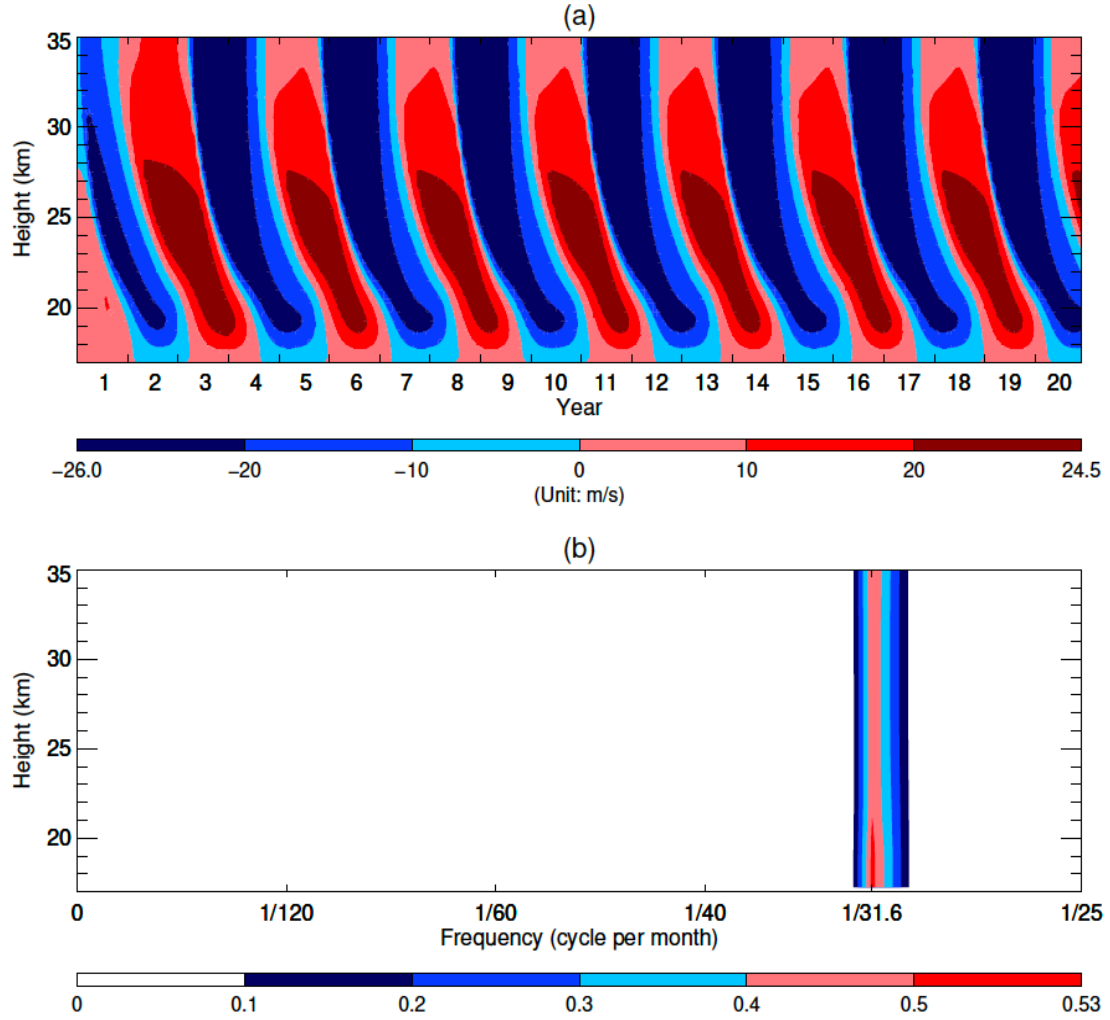


FIG. 5: (a) Same as FIG. 4a, but with the enhanced $\alpha(z)$ depicted as the red line in FIG. 1a. (b) Same as FIG. 4b, but for the doubled CO₂ Run.

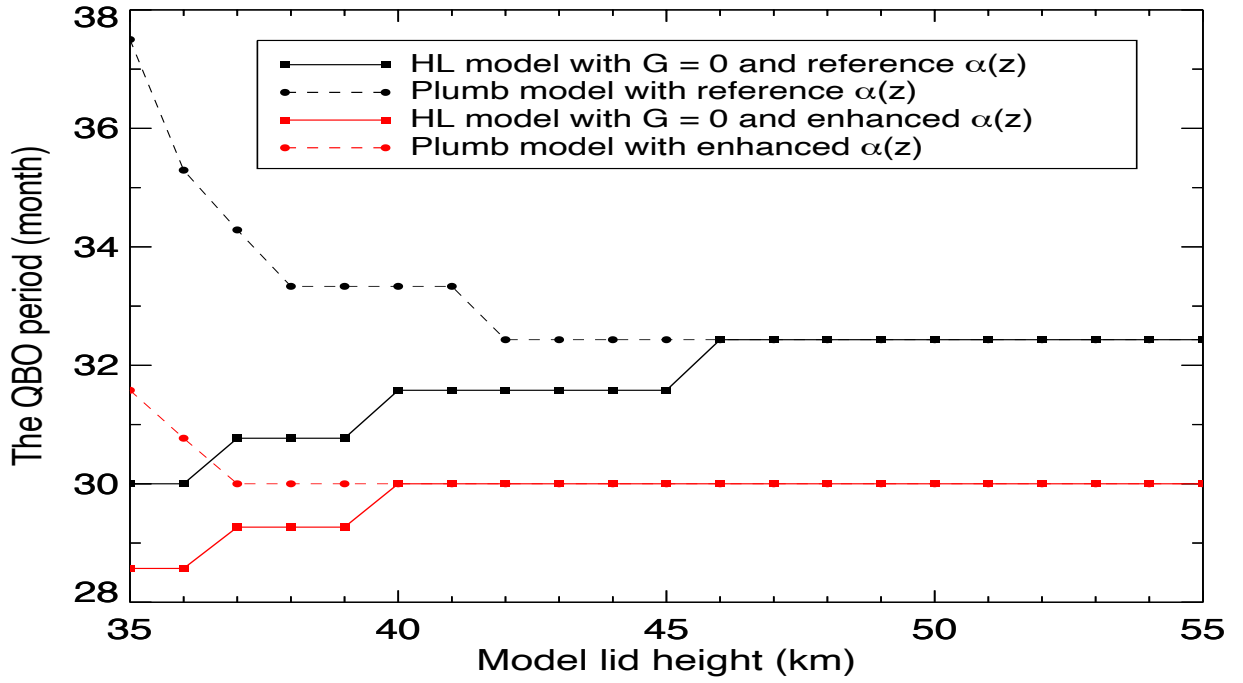


FIG. 6: The relationship between the simulated QBO period with the height of the model lid. Black and red lines depict the results from using the reference radiative damping and the enhanced radiative damping respectively while solid and dashed lines delineate the results from the HL model with $G = 0$ and the Plumb model respectively.